JWST Deep Imaging with MIRI: A mid-IR view of the Reionization Epoch.

H.U. Nørgaard-Nielsen (DTU)
L. Colina (CAB/CSIC, SPAIN)
G. Wright (UK-ATC)

On Behalf of the MIRI EC "High z Universe" team:

A. Alonso-Herrero, R. Azzolini, T. Boeker, B. Brandl, K. Caputi, D. Dicken, A. Eckart, M. García-Marín, J. Hjorth, S. Kendrew, O. Lefevre, A. Labiano, P. Perez-Gonzalez, J. Pye, T. Tikkanen, F. Walter, M. Ward, P. Van der Werf

Introduction to MIRI Capabilities for Deep Imaging - 1

MIRI 's unprecendented sensitivity in the mid-IR means it can provide critical data in the epoch of ionisation.

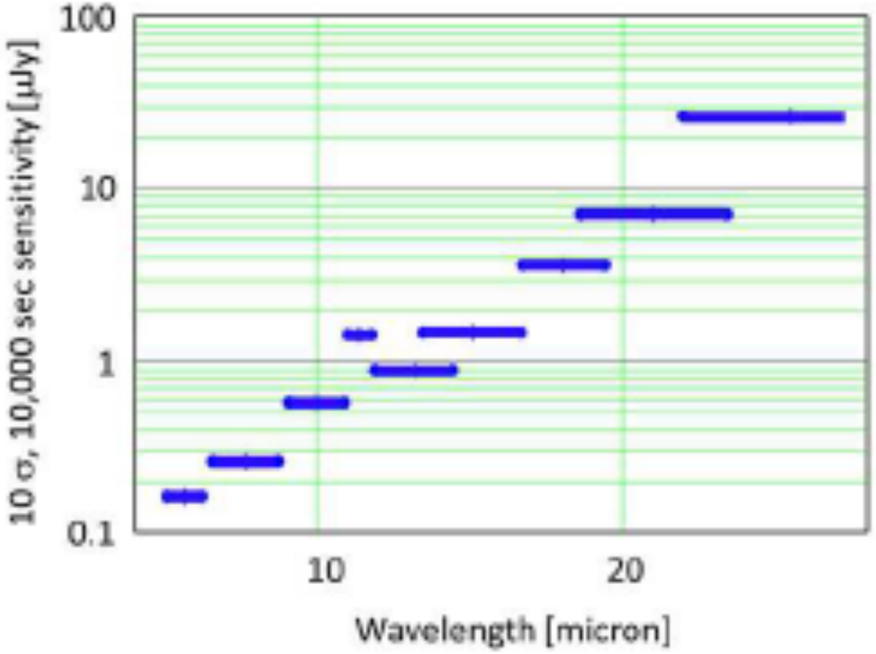

At long wavelengths MIRI sensitivity is limited by telescope background radiation

Therefore for deep imaging of very faint high redshift sources the filters at 5.6, 7.7, 10.0 and 11.3 microns are of most interest

Introduction to MIRI Capabilities for Deep Imaging - 2

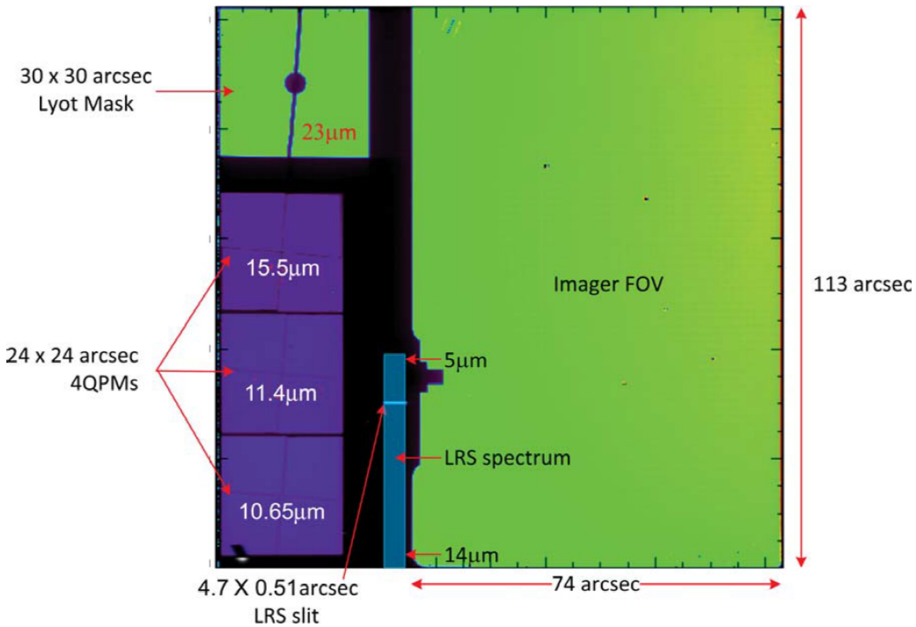

MIRI provides diffraction limited images of FWHM 0.32 arcsec at 10um sampled with 0.11 arcsec pixels

The field for imaging is 74x113 arcsec

To obtain the best sensitivity observations are taken using a pre-defined dither pattern

JWST instruments do not simultaneously image the same field

The relatively small field size of MIRI means that it is not well suited to wide area searches /surveys

MIRI is best used to study areas already well studied or follow-up known or suspected very high redshift sources to constrain their properties

Reionization Epoch: start: z ~ 1000 (CMB)   end: z ~ 6 (QSO)

Key issue: where are the ionizing photons coming from?

Most likely: low luminosity star forming galaxies
<luminosity> unknown

Need to push JWST + MIRI to the limit: Exploit Nature's own extremely large Telescope

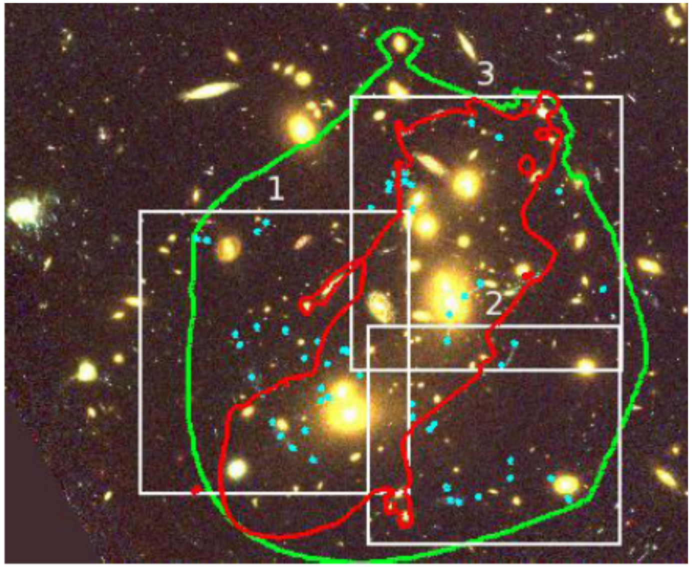

Figure 2. Color image of A2744 as obtained with HST/ACS (F435W+F606W+F814W). in green the enclosing region where we expect multiple images at $z = 7$, and blue circ modelling. Thin white lines delineate the regions shown in more detail in Fig. 3

Massive clusters: magnification by factors ≤ 40 of background galaxies

emphasize on intrinsically faint galaxies

unique feature for lensing cluster fields compared to blank fields (for the same investment in observing time)

Ex . Abell 2744

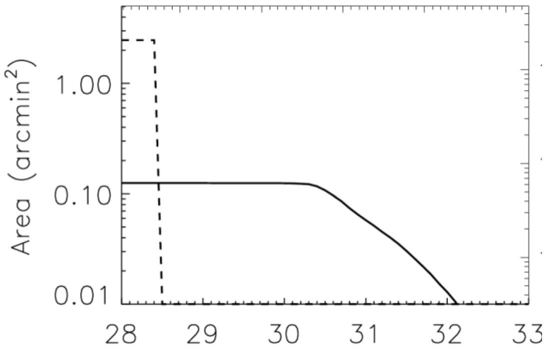

Richard et al. (2014) HFF clusters

Calibrating the HFF cluster lenses 19

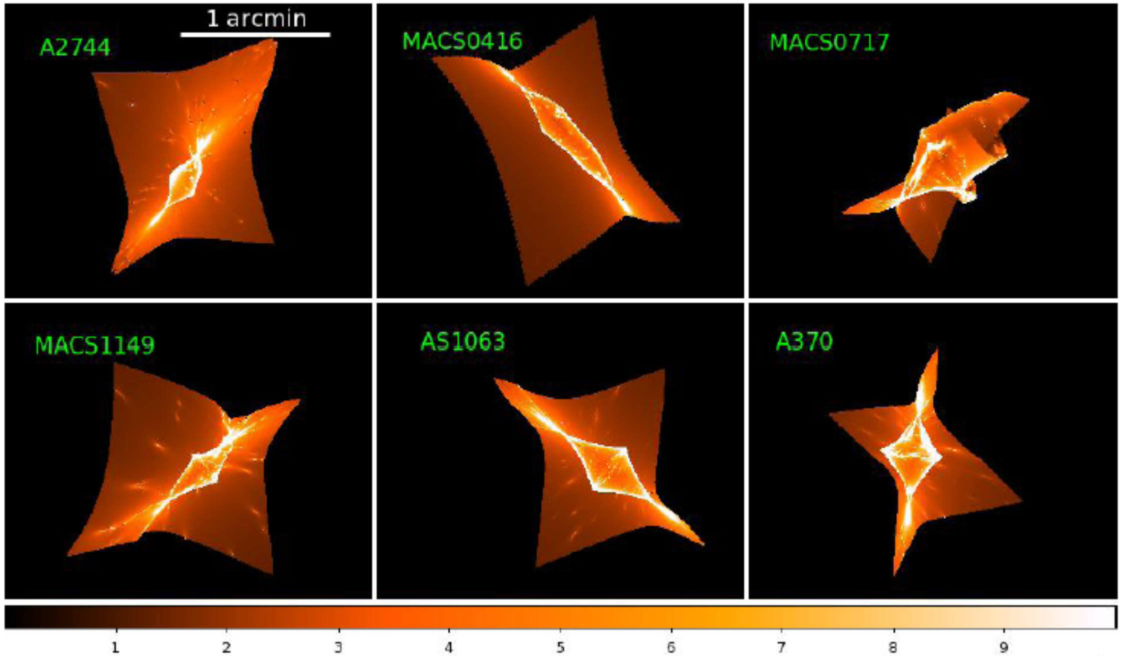

Magnification 0 -> 10

Figure 14. Source-plane magnification maps corresponding to the expected ACS+WFC3 coverage of the Frontier Field clusters. The color scale gives the magnification value.

HST Frontier Fields: ~140 orbits per cluster -> many more multiple images -> large improvement in lensing models -> accurate magnification maps and effective volumes

Strong emphasis on obtaining more spectroscopic redshifts

Atek et al. (2015)

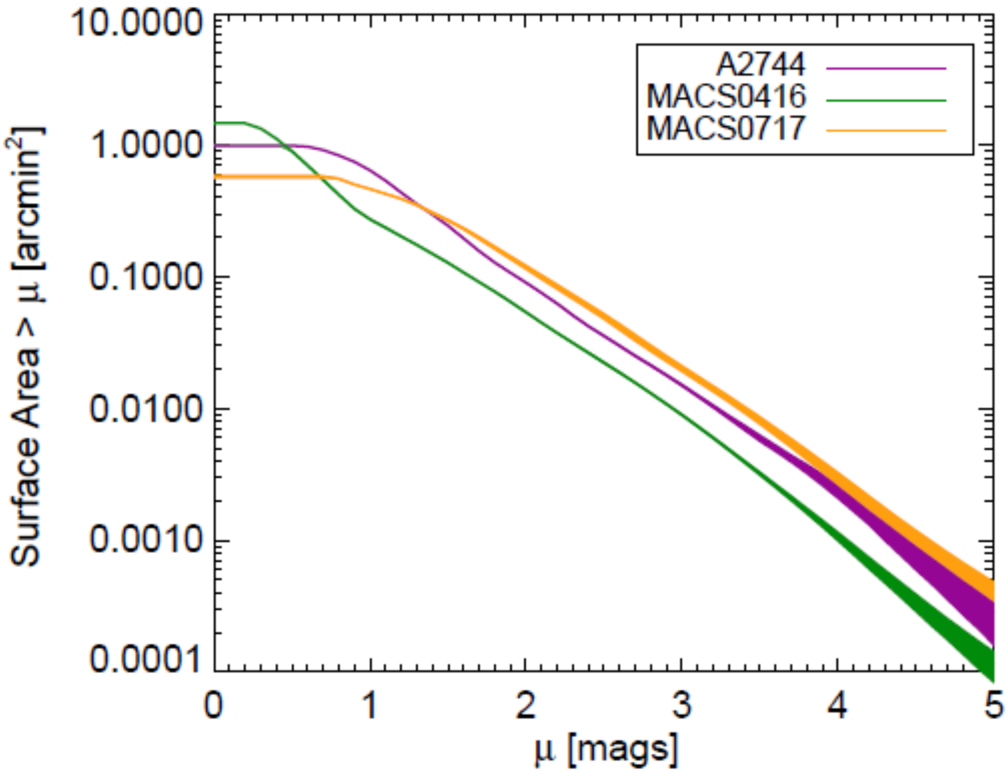

FIG. 4.— The cumulative surface area in the source plane at $z \sim 7$ as a function of the amplification factor (in magnitudes) derived from the mass modeling of the three HFF clusters. Uncertainties in the surface area are also shown at the 1-σ level .

Typical magnification:
1.0 – 1.5 mag

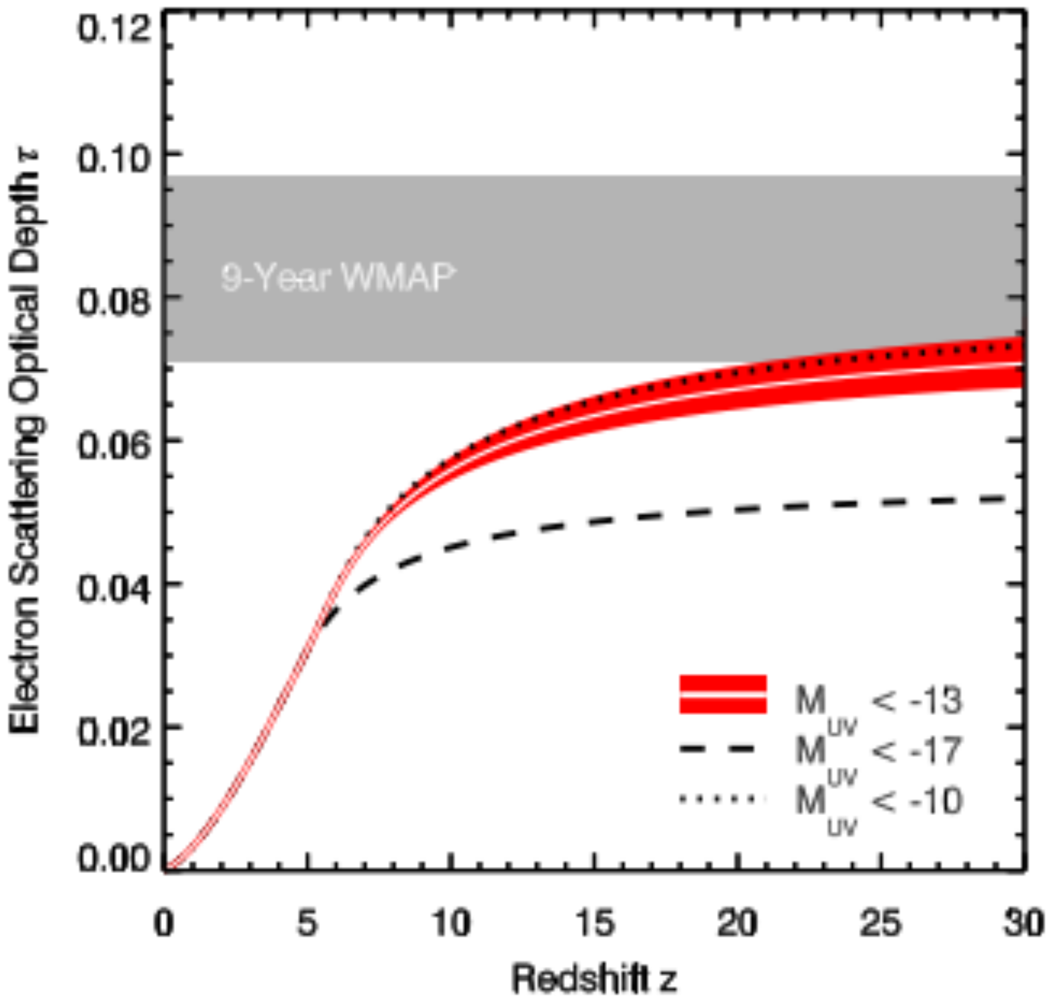

ontributions from galaxies with $M_{UV} < -17$ (maximum likelihood model show

<- Planck

<- Planck

<- available

Robertson et al. (2013

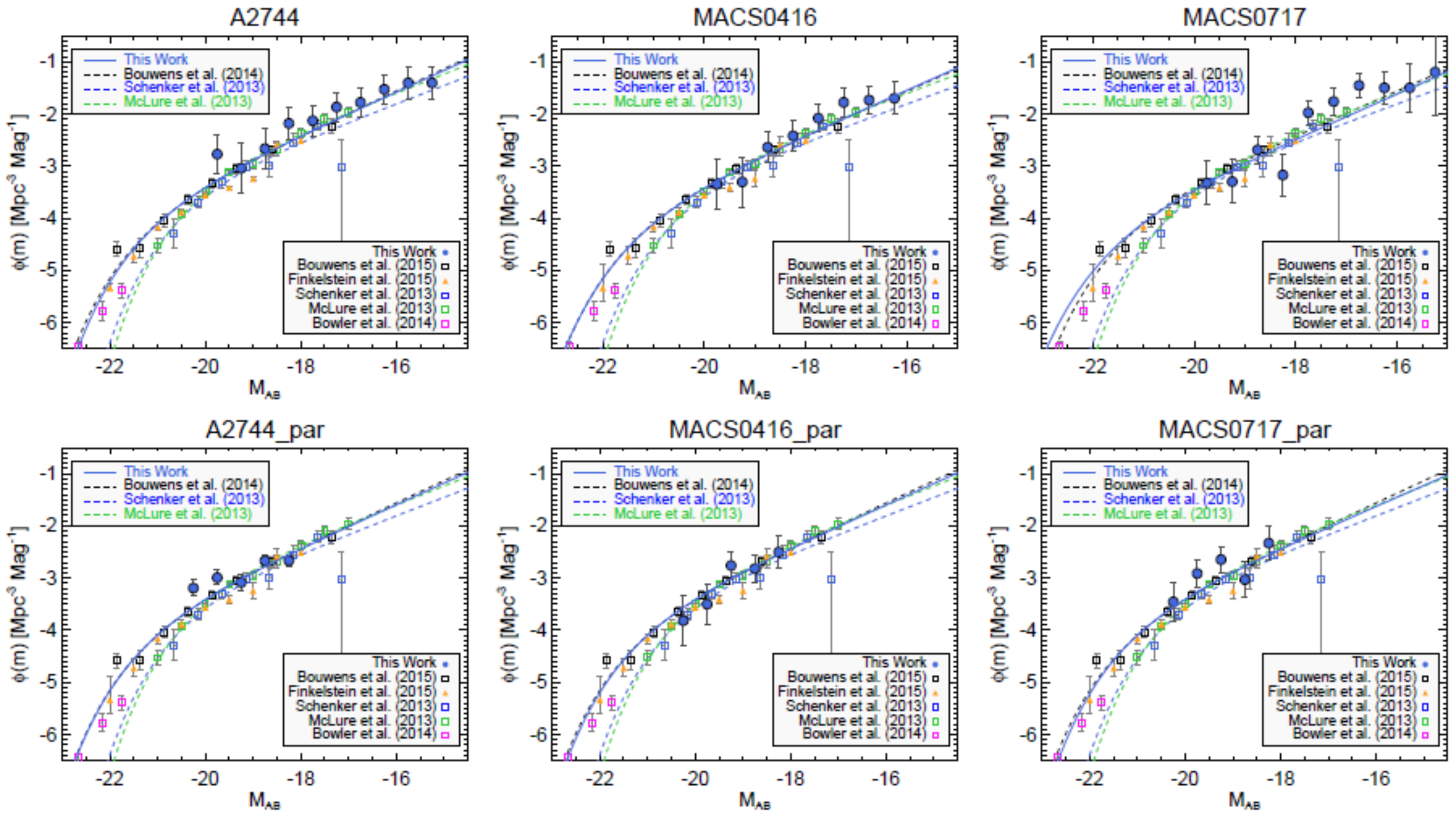

FIG. 7.— UV luminosity function at $z \sim 7$ computed individually in each field. The blue circles represent our determination with 1-σ uncertainties while the blue solid curve is our best Schechter function fit to the LF. We compare our results to previous literature results in blank fields. The black squares and dashed curve are from a compilation of *HST* legacy fields by Bouwens et al. (2014). We also show the LF determination of Schenker et al. (2013b, blue squares and dashed curve) and McLure et al. (2013, green squares and dashed curve) derived in the UDF12 field. We also include data points on the bright-end of the LF [magenta squares] from a wide area survey by Bowler et al. (2014).

Atek et al. (2015) z ~ 7 – 8 HFF

M_{AB} < -15 , Φ(m) increased for M_{AB} > -18

Main spectral features for high – z objects:

Lyα break -> redshift

Balmer jump and slopes ≤ 4000 Å

→ age

Very young population -> emission lines, UV slopes

Old star populations in high-z objects

e.g. Egami et al. 2005, Eyles et al. 2005, Richard et al. 2011, Zeng et al. (2012)

stellar population synthesis →

z ~ 6 stellar age ~400 – 500 mill yrs

→ 8 < z < 13 -> information about SFR at age(z) and previous epochs

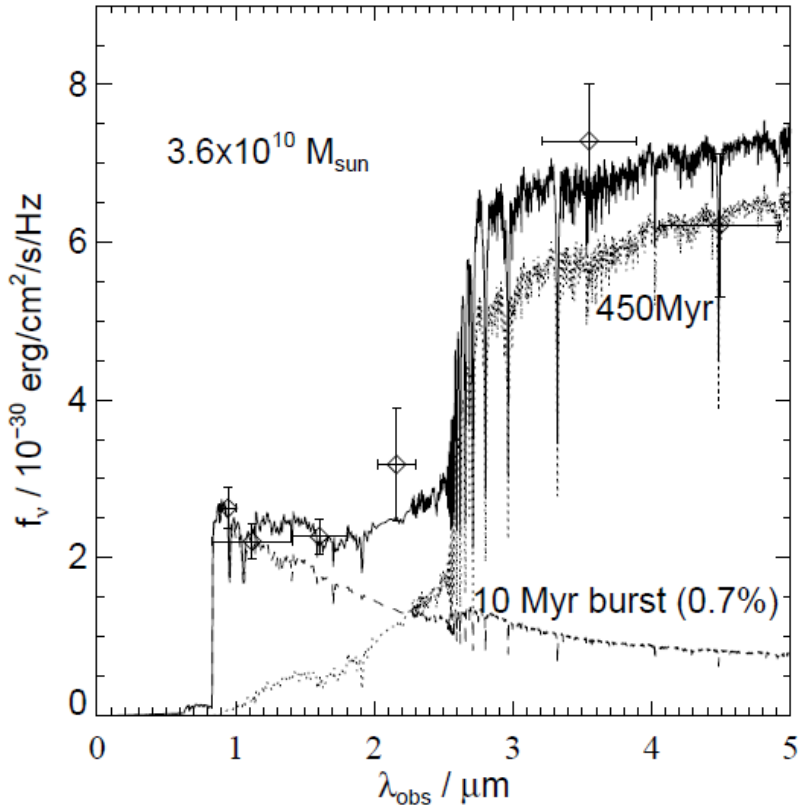

Figure 9. The best-fitting two-component stellar population model (Salpeter IMF) for SBM03#1: a dominant 450 Myr population of mass $3.6 \times 10^{10} M_{\odot}$, with some ongoing star formation activity (a burst for the last 10 Myr involving 0.7% of the stellar mass). Using a Chabrier IMF produces an identical best-fit age,

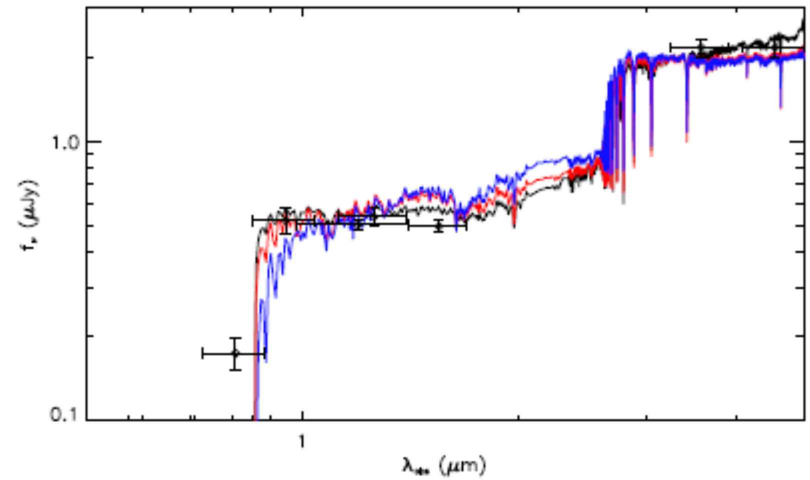

Figure 3. Observed SED of image 5.1 (black data points) and model templates. The black curve represents the best fit to the photometry (τ = 500 Myrs), whereas the blue/red curves show the best fit for younger but more punctuated star-formation histories (τ = 10/100 Myrs respectively), giving a poorer fit to the photometry

Eyles et al. (2005) z ~ 6

Richard et al. (2011) Abell 383, z ~ 6, μ ~ 11

Zeng et al. (2012) MACS1149-JD1: z = 9.6 ±0.2, μ ~ 14, age ~ 500 Myr

Age ~500 Myr -> z(stellar pop) > 11.3

Bright object !

->

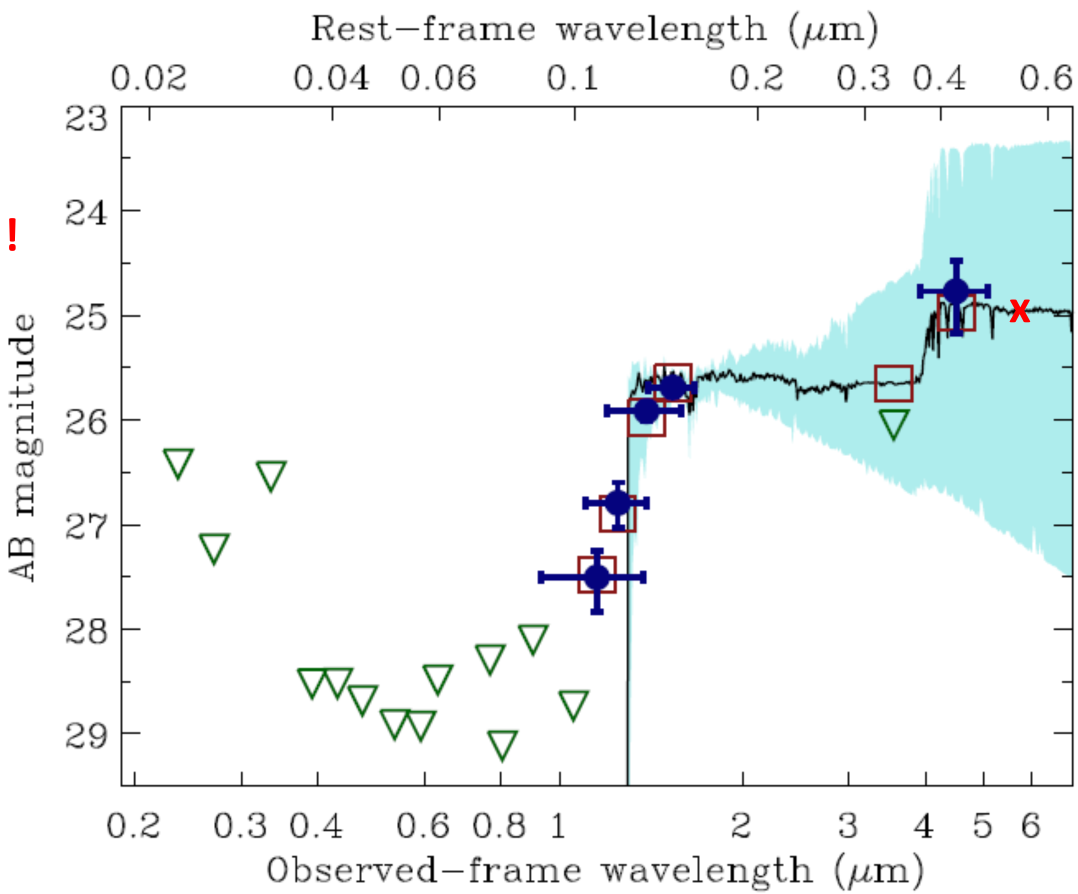

MIRI

x 5.6 7.7μm

MIRI capability for constraining stellar population models for high z sources

Figure 4 – Stellar population synthesis modeling results for MACS1149-JD1.

Justification for MIRI/JWST

MIRI has unique sensitivity > 5 µm, complementing the sensitivity of NIRCam at lower wavelengths

NIRCam? F440W clean Balmer jump: $z < 9$, $z > 9$ MIRI

To obtain SED's to constrain stellar mass and reddening: coverage restframe > 0.7µm required ->

NIRCam	$z \lesssim 5$
MIRI 5.6µm	$z \lesssim 7$
MIRI 7.7µm	$z \lesssim 10$

To discover First Light Objects: a key science goal for JWST

Single First Light Object very faint even for NirCam

Primodial gas Z = 0 (POP III)

First Light stars formed in 105 – 10**6 Mo dark halos, mass > 100 Mo, z = 20 – 50**
Lifetime a few mill. Yrs

POP III galaxies formed in 107 – 10**8 Mo dark halos, z ≤ 15**

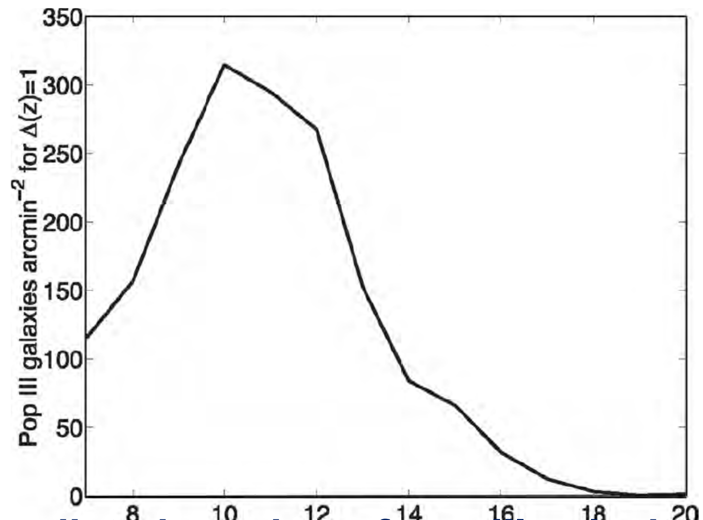

The predicted number of pop III galaxies per square arcmin (Zackrisson et al. 2012).

Zackrisson et al. (2012)
POP III galaxies(z) based on Trenti et al. (2009) dark halo simulations and detailed modeling of formation, spectral evolution etc

Zackrisson et al. (2011) Yggdrasil (Tree of Life!) spectral analysis code -> color criteria for selecting Pop III galaxies

Combination of MIRI and NirCam:
m(560) – m(770) <-> m(444) – m(560)

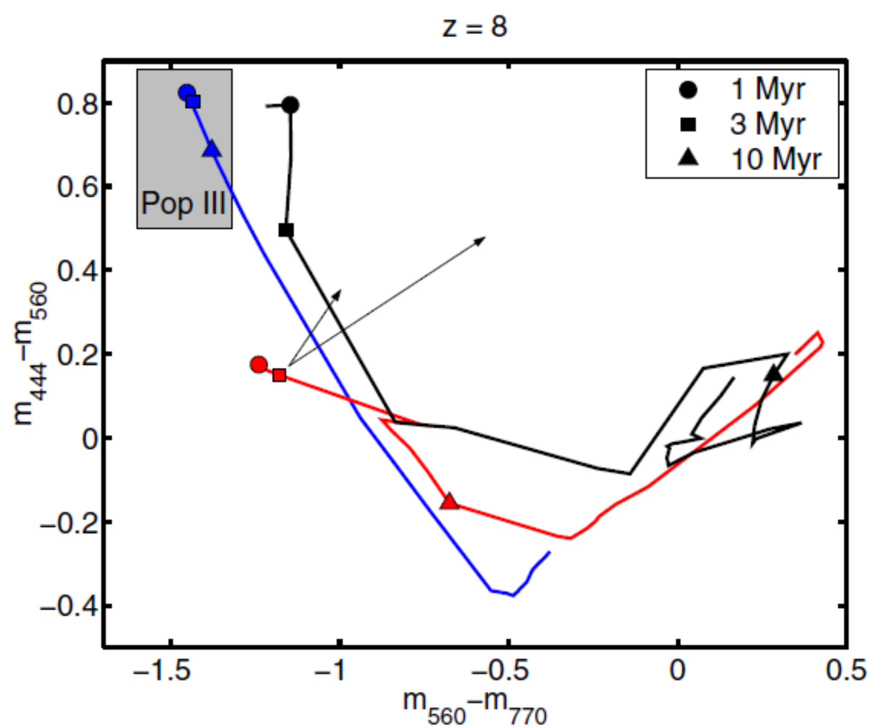

ïgure 8. Signatures of type A, Pop III galaxies in the $m_{560} - m_{770}$ vs. $ı_{444} - m_{560}$ diagram at $z = 8$. The lines correspond to a limited set of the nstantaneous-burst models presented in Figure 7 (to avoid cluttering): Pop III.2 blue line), Pop II (red line), and Pop I (black line). Markers along the tracks

Z = 8

Follow-up spectroscopy of brightest objects will be needed

Capability of MIRI for deep Imaging:
Ex. assuming 20 h observing available ->

limit AB 27.9 (<5.6μm, 7.7μm>, 4 σ) can be obtained supplemented with NIRCam photometry

Expected number of sources detected

Richard (2015) based on Atek et al.(2015) luminosity function

numbers for 3 cluster and 2 blank fields

DROP-FIL T	Z - INTERVAL	BLANK	CATS	3L + 2B
F070W	4.9 - 6.3	26.3	19.6	111
F090W	6.3 - 8.3	19.0	15.1	84
F115W	8.3 - 10.5	10.6	9.1	49
F150W	10.5 - 12.5	5.3	5.0	26

The 5 x 20 h deep MIRI observations will also detect a lot of low – redshift objects (z < 6)

> 1000 sources 2.0 < z < 4.9
~ 100 sources 4.9 < z < 6.3

Galaxy sizes: strong evolution with z

Kawamata et al. (2015)

MIRI 6 - 8 µm imaging ->

first time direct high resolution obs (6 times better than Spitzer) ->

morphology of the older (> 100 Myr) stellar populations

Unique for establishing the relationship between assembly of the stellar mass and size growth for z > 3

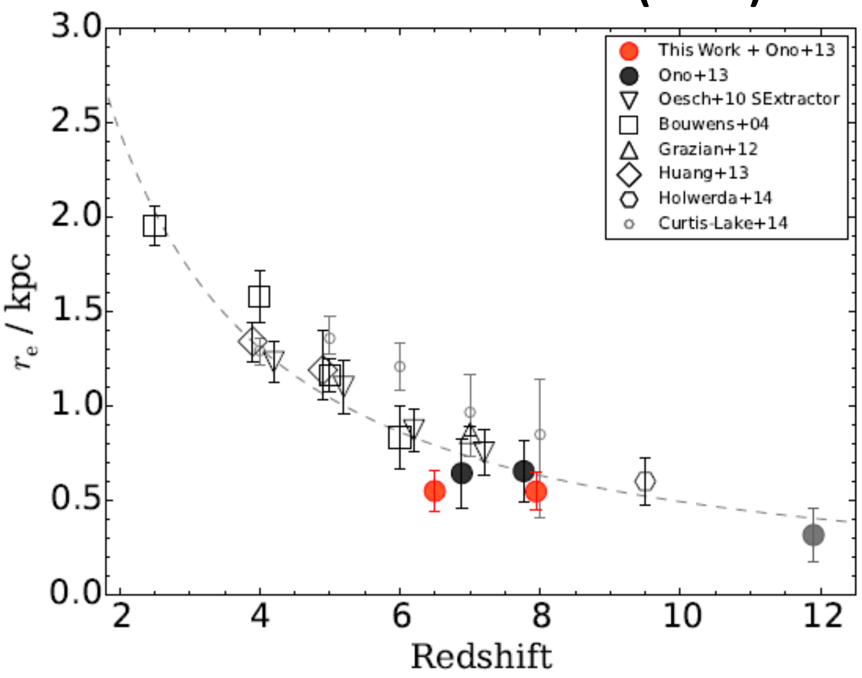

Figure 6. Redshift evolution of the average size of bright galaxies. The red circles show the weighted-average radii of our samples combined with Ono et al. (2013)'s, while the black circles are for Ono et al. (2013)'s. The error bars show the 1σ standard error.

Star formation peaks z ~1
Galaxy mass distribution expected to skrew ->
low mass objects by z ~5

Reliable mass estimates require obs at
~1.5 µm -> ~8 µm at z ~ 5

MIRI enables obs: 3 < z < 6

-> faint end of mass function
z ~ 3: ~10**8 Mo
z ~ 6: ~10**9 Mo

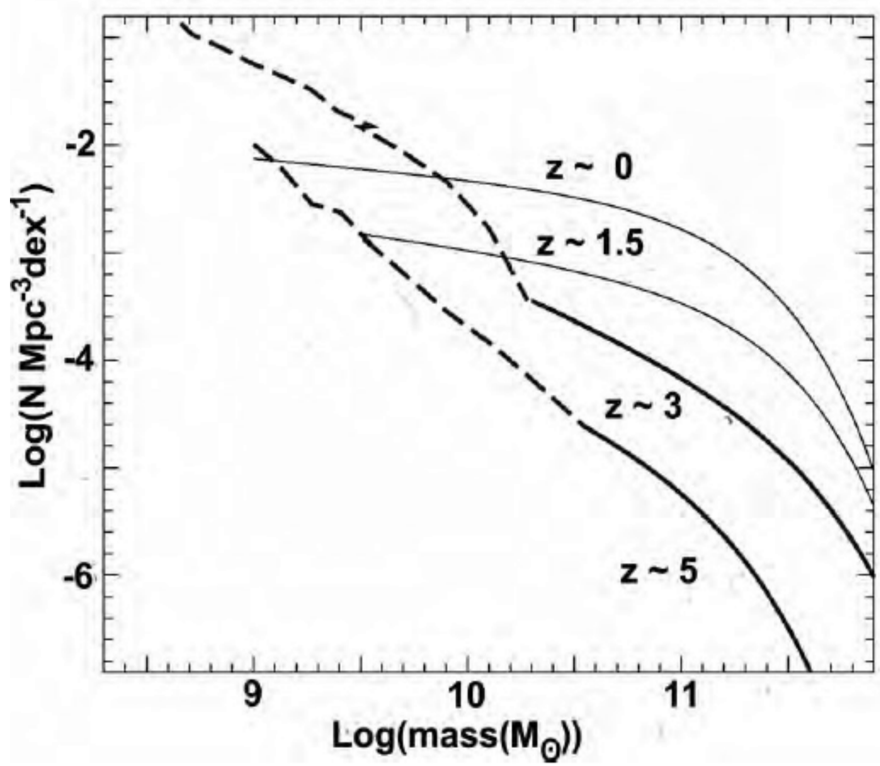

- **Evolution of galaxy mass function with redshift (Caputi et al 2011)**
  - Solid lines, deepest IRAC images (confusion ltd)
  - Dotted – MIRI [5.6]=27

Deep MIRI imaging will provide unique information needed for our understanding of the details of the Reoinization Epoch e.g.

the stellar populations in the sources responsible for the ionizing photons

stellar masses, morphology and reddening of intermediate redshift objects.

Identification of Z = 0 Objects

For More detailed information about MIRI capabilities:

Posters by :

Glasse et al: Modelling of the Performance of JWST MIRI (M 3)

Garcia-Marin et al: Observing nearby galaxies with MIRI, Challenges and Optimization (GA 29)

and

PASP Volume 127, Issue 953 (2015) available at http://ircamera.as.arizona.edu/MIRI/index.htm

Robertson et al. (2014)